Published in Metall. Mater. Trans. A, 33A (2002) 1779-1794

On DTA Curves for the Melting and Freezing of Alloys

W.J. Boettinger and U.R. Kattner
Metallurgy Division
NIST
Gaithersburg, MD 20899,U.S.A.

Abstract

Using a heat flow model of a DTA (differential thermal analyzer) and thermal characteristics obtained by fitting experimental results for a pure metal, the response of the DTA is modeled for the melting and solidification of alloys. The enthalpy-temperature relation used for the alloy simulations is obtained by two different methods: 1) equilibrium and Scheil considerations derived solely from thermodynamic information and 2) solute diffusion micromodels coupled to the DTA heat flow equations. During the consideration of pure material melting, simple expressions are obtained for the effect of sample size and heating rate on the DTA melting onset temperature, peak temperature and peak height that assist in the proper calibration of a DTA. For alloys, the smearing effect of the DTA heat flow at different heating and cooling rates is demonstrated for various solidification path features. In particular, the DTA peak temperature during melting, which is often selected as the liquidus temperature experimentally, is shown to be significantly higher than the liquidus temperature for small freezing range alloys and/or for alloys with slow solid diffusion. DTA curves calculated for freezing with dendritic growth due to supercooling quantify the errors associated with of the determination of the liquidus temperature on cooling.

Keywords: differential thermal analysis (DTA); computer simulation; thermal properties; kinetics

I. Introduction

DTA (differential thermal analysis) measurements are a standard method of determining transformation temperatures of materials[1]. Accurate interpretation of these measurements is essential when they are used to infer the location of equilibrium phase diagram boundaries. The accuracy of the measurements is affected by the details of heat transfer within the measurement cell and by transformation kinetics. Simulations can provide understanding into how thermal events from transformations are reflected in the DTA signal and can enable more accurate interpretation of DTA results from samples with unknown characteristics. While theoretical treatments and analysis of measurements from DTA and other thermo-analytical methods are not new[2-15], errors of interpretation continue to filter through the scientific literature and industrial technology. It is timely to re-examine these theoretical treatments and couple them with recent progress in alloy thermodynamic descriptions and solidification models.

Many early theoretical treatments of DTA were focused on the optimization of apparatus configuration. Heat exchange is analyzed between the various parts of the apparatus; viz., sample, reference material, containers, thermocouples, and furnace. The major difference between the various analyses is the number of parts that are considered and whether radiation, conduction and convection are distinguished for the heat exchange. The heat flow between various objects in the system is typically modeled using systems of ordinary differential equations (ODE). These methods assume that a single temperature can represent each of the different parts of the system. One exception to this approach, Banerjee et al.[2], used a FEM (finite element method) analysis of the temperature distribution within the parts of a DTA that also included radiation view factors. Cunningham and Wilburn[3] included heat loss along the thermocouple wires in their very detailed treatment. In addition to DTA, Gray[4] applied the analysis to power-compensation DSC (differential scanning calorimetry) and TGA (thermogravimetric analysis). Heyroth[5] developed

the apparatus function for DTA that included radiation and convection in order to explain the heating rate dependence of the time constants. Shull[6] showed that heat flow between sample/cup and cup/wall resulted in an offset between the temperatures of the beginning of the deviation from the baseline in the DTA curve and the actual temperature of an invariant reaction.

Within the sample, early work focussed on deriving an expression for the heat of reaction[7] or determining the factors affecting the DTA peak shape, such as sample aspect ratio[8]. Kissinger[9] used homogeneous reaction kinetics for the analysis of peak shape. This treatment was later expanded by Meisel and Cote[10] for heterogeneous reaction kinetics. Examples of analysis of other kinetic factors can be found in the work of Ozawa[11] (non-isothermal diffusion), Flynn[12] (reaction kinetics) and Perepezko[13] (nucleation and growth). Fredriksson[14,15] presented analyses of different solidification behavior, comparing results to equilibrium (lever) and Scheil solidification models, which represent the two limiting cases for solidification[16]. Recently Opfermann[17] has developed software to fit thermal analysis data with a sizeable number of reaction types. None seems appropriate to melting and solidification of metals and alloys where interface attachment kinetics can usually be ignored.

Wu and Perepezko[18] recently showed that using the peak temperature during melting in a DTA failed to give a reliable liquidus temperature for two important commercial Ni-base alloys. The experiments used small 180 mg samples heated at 20 K/min. Despite using careful calibration procedures for the high heating rates, only interrupted cycle experiments were able to reveal the true liquidus temperature. This temperature was determined to be more than 20 K lower than the DTA peak. The cause of such difficulty was unclear. Several authors used direct immersion of the thermocouple in Al alloy[19,20] and solder melts[21]. Certainly, the direct immersion of thermocouples is known to avoid many defects of the DTA instrument and is preferable when thermocouple reaction can be avoided.

We first present a model and its analytical solution for the melting of a pure element. When combined with experimental DTA data for a pure metal at various heating rates, this solution provides a method to determine the response times of the instrument. Numerical solution of the model is then obtained for an arbitrary enthalpy-temperature function such as can be obtained from a thermodynamic analysis of multicomponent phase equilibria. Finally we include the possibility that the enthalpy temperature behavior of the sample is time dependent through the inclusion of a solid diffusion model in the melting solid during heating and a dendritic solidification model during cooling.

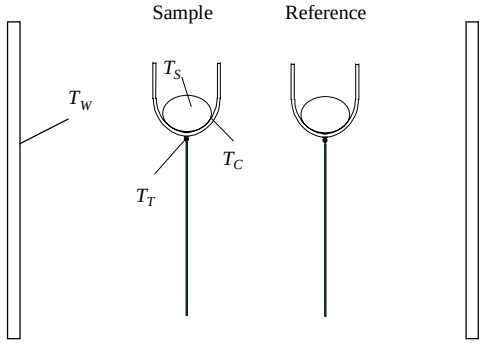

Fig. 1 Schematic of DTA geometry (not to scale).

II. Heat Flow Model

We employ an ODE based approach. Figure 1 shows a typical DTA geometry where $T_S(t)$, $T_C(t)$, $T_T(t)$ and $T_W(t)$, the sample, sample cup, thermocouple and furnace wall temperatures are noted. A similar set of variables can be used to describe the temperatures of the reference sample, cup and thermocouple. In Appendix A, a system of ODE's that describes these six temperature is given. For this paper we use a reduced set that employs several simplifications. We only consider heat flow: a) between the sample and the sample cup; b) between the sample cup and the furnace wall; and c) from the sample cup to the thermocouple. We neglect small heat flow from the thermocouple back to the sample cup and heat flow from the thermocouple tip to the thermocouple support rod as appropriate for a well designed DTA. We also neglect heat flow between the sample and reference cups. Examination of experimental temperature-time data (described below) for the reference thermocouple during the melting of small (180 mg) samples of pure Ni at 5 K/min show less than 0.8 K variation from linearity. This indicates that very little heat flows between the reference and sample cups in these experiments. Including the heat flow between the two cups is important whenever the temperature difference between the two cups becomes large. This would be most likely for the melting of pure materials at high heating rates with large mass or heat of fusion. For cooling DTA, large supercooling and rapid solidification would cause large temperature differences to develop.

For the simple case, we let $h_{S,C}A_{S,C}$, $h_{W,C}A_{W,C}$, and $h_{T,C}A_{T,C}$ be the products of the heat transfer coefficients $h_{X,Y}$ and areas $A_{X,Y}$ for the heat flow a), b), and c) described above, respectively. Because we will lump these various heat transfer parameters in to response times, an exact physical interpretation of area is not necessary.. We also let m_S and H_S be the sample mass and enthalpy/unit mass, m_C and C_p^C be the crucible mass and heat capacity/mass and m_T, and C_p^T be the thermocouple mass and heat capacity/mass. (See *Nomenclature* at the end of the paper).

A heat balance gives

$$\begin{cases} m_S \dot{H}_S = \dfrac{m_C C_p^C}{t_{S,C}}(T_C - T_S) \\ \dot{T}_C = \dfrac{1}{t_{S.C}}(T_S - T_C) + \dfrac{1}{t_{W,C}}(T_W - T_C) \\ \dot{T}_T = \dfrac{1}{t_{T,C}}(T_C - T_T) \end{cases} \qquad [1]$$

where the dot represents time differentiation. The instrument time constants $t_{S,C}$, $t_{W,C}$ and $t_{T,C}$ are given by

$$\begin{cases} t_{S,C} = m_C C_p^C / h_{S,C} A_{S,C} \\ t_{W,C} = m_C C_p^C / h_{W,C} A_{W,C} \\ t_{T,C} = m_T C_p^T / h_{T,C} A_{T,C} \end{cases} . \qquad [2]$$

The parameter, $t_{S,C}$ is the characteristic response time for heat flow between the metal *sample* and the crucible *cup*; $t_{W,C}$ is the response time between the furnace *wall* and the *cup*; and $t_{T,C}$ is the response time between the *thermocouple* and the *cup*. We will assume that these response times are independent of temperature. It is possible with numerical solutions to easily add radiation and/or temperature dependent heat transfer coefficients However, this and other generalizations require the use of more adjustable parameters in the model. As seen below even with these assumptions, the model successfully simulates the DTA signal of the melting of pure Ni. We will further assume that the furnace heating rate[*], α, is constant such that the interior furnace *wall* is given by

[*] Some heat flux DSC (differential scanning calorimeter) instruments employ the reference thermocouple as the control thermocouple for the furnace. In this case one would assume that the reference thermocouple increases linearly with time. The furnace wall temperature would become an unknown in the system of equations. In the case where heat flow between sample and reference cup can be neglected, the two situations are identical.

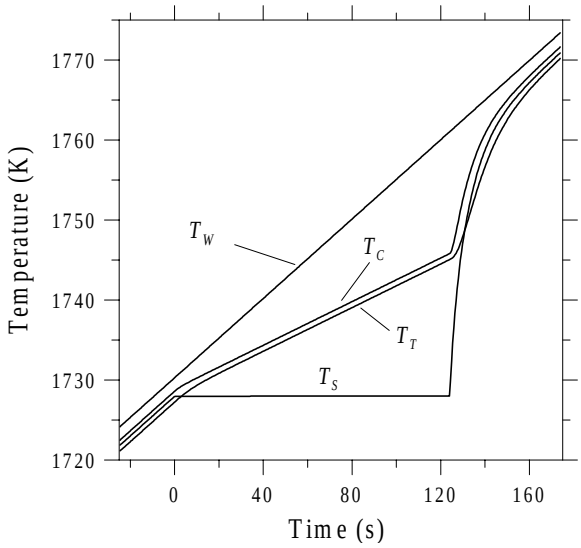

Fig. 2. Plot of calculated sample, sample cup, sample thermocouple and furnace wall temperatures vs. time curves for melting of 180 mg sample of pure Ni at 15 K/min.

$$T_W(t) = \text{constant} + \alpha t \quad . \qquad [3]$$

For situations where transformation kinetics can be ignored, the enthalpy is only a function of temperature and

$$\dot{H}_S = \frac{dH_S}{dt} = \frac{dH_S}{dT_S}\frac{dT_S}{dt} = H'(T_S)\dot{T}_S \quad . \qquad [4]$$

Inclusion of kinetic effects produce a time dependent sample enthalpy function that will be considered in Section V.

III. DTA Signal for Melting of Pure Material

A. Analytical Solution

An analytical solution for the melting of a pure material can be found. We pick $t = 0$ as the initiation of melting in the sample and $t = t_M$ as the termination of melting in the sample. The solution must be computed differently for the three time regimes: $t < 0$, $0 < t < t_M$, and $t > t_M$. Let T_M be the sample melting point, L be the heat of fusion/unit mass and C_p^{S0} be the heat capacity/unit mass prior to melting. The furnace wall temperature is assumed to follow Eq. [3], throughout the three time regimes.

Prior to melting ($t < 0$) and after an initial transient, the temperature solutions to Eq. [1] are all linear in time, with the same slope α, but with different offsets:

$$\begin{cases} T_S = T_M + \alpha\, t \\ T_C = T_M + \alpha\,(t + t_S R) \\ T_T = T_M + \alpha\,(t + t_S R - t_{TC}) \\ T_W = T_M + \alpha\,(t + t_{S,C} R + t_{W,C} R + t_{W,C}) \end{cases} \quad [2]$$

where the ratio of the total heat capacity of the sample prior to melting and the cup, R, is given by

$$R = m_S C_p^{S0} / m_C C_p^{C} \quad . \quad [3]$$

At a given time, the furnace wall temperature is highest, followed by the cup and the sample. For the instrument described below, the sign of the quantity $[t_{S,C} R - t_{T,C}]$ is negative and thus the thermocouple temperature is lower than the sample temperature (Figure 2). The size of all temperature offsets are proportional to the heating rate.

During melting, $0 < t < t_M$, the sample temperature is assumed constant, $T_S(t) = T_M$. The ODE for T_S is not solved. The three temperatures are given by:

$$\begin{cases} T_S = T_M \\ T_C = T_M + \alpha R t_{S,C} + \dfrac{t_{S,C}}{t_{S,C} + t_{W,C}} \alpha t \\ \quad + \dfrac{t_{S,C} {t_{W,C}}^2 \alpha}{(t_{S,C} + t_{W,C})^2} \left\{ 1 - \exp\left[-\left(\dfrac{1}{t_{S,C}} + \dfrac{1}{t_{W,C}} \right) t \right] \right\} \\ T_T = T_M + \alpha R t_{S,C} - \alpha t_{T,C} + \dfrac{t_{S,C}}{t_{S,C} + t_{W,C}} \alpha t \\ \quad + \dfrac{{t_{S,C}}^2 {t_{W,C}}^3 \alpha}{(t_{S,C} + t_{W,C})^2 (t_{S,C} t_{W,C} - t_{S,C} t_{T,C} - t_{W,C} t_{T,C})} \\ \quad \times \left\{ 1 - \exp\left[-\left(\dfrac{1}{t_{S,C}} + \dfrac{1}{t_{W,C}} \right) t \right] \right\} \\ \quad - \dfrac{t_{W,C} {t_{T,C}}^2 \alpha}{t_{S,C} t_{W,C} - t_{S,C} t_{T,C} - t_{W,C} t_{TC}} \left\{ 1 - \exp\left[-\left(\dfrac{t}{t_{T,C}} \right) \right] \right\} \end{cases} \quad . \quad [7]$$

During this regime both the cup and thermocouple temperature-time curves exponentially approach linear behavior with a slope of $\alpha\, t_{S,C} / (t_{S,C} + t_{S,W})$ as shown in Figure 2.

The melting time (t_M) can be obtained by substituting the solution for $T_C(t)$ into Eq. [1] (top) and integrating from zero to t_M. The value of t_M is the root of the equation

$$t_M^2 + 2 \frac{{t_{W,C}}^2 + R(t_{S,C} + t_{W,C})^2}{(t_{S,C} + t_{W,C})} t_M - \frac{2 t_{S,C} {t_{W,C}}^3}{(t_{S,C} + t_{W,C})^2} \left\{ 1 - \exp\left[-\left(\frac{1}{t_{S,C}} + \frac{1}{t_{W,C}} \right) t_M \right] \right\} - \frac{2(t_{S,C} + t_{W,C}) m_S L}{\alpha\, m_C C_p^C} = 0 \quad . \quad [8]$$

For all practical cases, $(1/t_{S,C} + 1/t_{W,C})\, t_M >> 1$, the exponential term can be dropped and

$$t_M = \sqrt{ \frac{2 m_S L (t_{S,C} + t_{W,C})}{\alpha\, m_C C_p^C} + \left[\frac{{t_{W,C}}^2 + R(t_{S,C} + t_{W,C})^2}{t_{S,C} + t_{W,C}} \right]^2 } - \frac{{t_{W,C}}^2 + R(t_{S,C} + t_{W,C})^2}{t_{S,C} + t_{W,C}} \quad [9]$$

or

$$t_M \approx \sqrt{ \frac{2 m_S L (t_{S,C} + t_{W,C})}{\alpha\, m_C C_p^C} } \quad . \quad [10]$$

Using the values for the response times determined below (selected values, Table I), the melting times numerically calculated with the three expressions (Eqs. [8] through [10]) for a heating rate of 15K/min are 124.00 s,123.96 s,and130.91 s, respectively. Thus the approximations are quite reasonable. The approximates inverse square root dependence on heating rate in Eq. [10] is due to the fact that the temperature difference between sample and cup increases linearly with time after the initiation of melting.

For $t > t_M$, the sample, sample cup and thermocouple return exponentially with time to the linear temperature behavior obtained during the first regime $t < t_M$. The solution is given in Appendix B and involves sums of terms, $\exp(r_i\, t)$, with inverse time constants r_i (Figure 2).

For DTA instruments, the 'DTA signal' is the difference between the sample and reference thermocouple temperatures. This difference is displayed vs. time or vs. a temperature. Some instrument software packages use the sample thermocouple temperature while others use the reference thermocouple temperature for the x-axis of DTA plots. The Perkin Elmer DTA 1700 instrument• used for the present paper, uses the sample

• Commercial products are referenced for completeness. Such identification does not imply recommendation or endorsement by the National Institute of Standards and Technology, nor does it imply that these products are necessarily the best available for the purpose.

Table I. Summary of Parameters for Pure Ni Calculations

Nominal Heating Rate (K/min)	Actual Heating Rate, α (K/s)	m_S (g)	$t_{S,C}$ (s)	$t_{W,C}$ (s)	$t_{T,C}$ (s)
5 (0.833 K/s)	0.081	0.184	5.88	4.74	5.52
10 (0.167 K/s)	0.163	0.186	5.47	4.69	6.37
15 (0.25 K/s)	0.248	0.177	5.32	4.57	6.0
Selected values			5.67	4.65	5.5

$m_C C_p^C$ = 0.257 J/K
C_p^S = 0.661 J/(g K), $T<T_M$
C_p^S = 0.734 J/(g K), $T>T_M$
L = 299 J/g
T_M = 1728 K
R = 0.49 (average sample mass and solid/liquid heat capacity)

thermocouple temperature, although it is a simple matter to extract the data for alternate plots.

For the simple heat flow model presented here, an alternate DTA signal is used. Because the heat flow between the sample and reference side of the DTA cell is neglected, the reference thermocouple temperature is always linear with time. Thus the difference between the sample thermocouple temperature and the *wall* temperature; *i.e.*,

$$\Delta T = T_T - T_W \qquad [11]$$

will only have a different baseline value than would the instrument due to the constant temperature offset between wall and reference temperatures. In all other respects (amplitude) the signal would be the same. The parameter ΔT can be considered either a function of time $\Delta T(t)$ or of sample thermocouple temperature $\Delta T(T_T)$. Properties of the DTA signal derived from the analytical solution will be given in Section III-D.

B. Numerical Solution

Because the analytical solution is cumbersome even for the pure material, and to simulate complicated alloy behavior, numerical solutions to the ODE's are useful. Fortunately systems of ordinary differential equations can be easily solved by various desktop software packages readily available to DTA users. Using the furnace wall temperature given by Eq.[3], the system of ODE's (Eq. [1]) is solved using MATHEMATICA*. For the numerical solution initial values must be specified for the three temperatures well below the melting point. In general, the results include an initial transient as the three temperatures adjust from their initial values and approach steady state prior to melting. The initial transient will not be discussed further.

* MATHEMATICA is a trademark of Wolfram Research, Inc., Campaign, IL 61820, USA.

C. Determination of time constants from data for melting of pure Ni

The measurements were performed with 0.9999 mass fraction purity Ni at nominal heating rates of 5 K/min, 10 K/min and 15 K/min. Enthalpy-temperature data for pure Ni were obtained from the SGTE data bank[22]. The $H_S(T_S)$ function is expressed as a single function of temperature by connecting the solid and liquid branches of the enthalpy curves using a hyperbolic tangent function with a 0.1 K width centered at T_M. The equivalent heat of fusion and heat capacities above and below T_M are given in Table I. Also given in Table I are the measured values of sample mass, heating rate (taken from the measured reference thermocouple temperature vs. time data). The cup heat content parameter, $m_C C_p^C$, is the sum of the products of the individual masses and heat capacities of the alumina cup and platinum cup holder.

Using a maximum time step of 0.05 s, the numerical calculations agreed with the analytical solutions (i.e., the melting times agreed to within 1 %). Thus, the numerical solution was used to fit the experimental data in an automated procedure. The mean square deviation of the $T_T(t)$ numerical solution from the $T_T(t)$ data was minimized by iterating the values of $t_{S,C}$, $t_{W,C}$ and $t_{T,C}$ that were used as input to the ODE solver. The best fit values for each heating rate are given in Table I. The small decrease in the time constants $t_{S,C}$ and $t_{W,C}$ with increasing heating rate may indicate the minor need to include radiation terms in the governing equations. However for the present paper, this effect will be neglected and a fixed set of time constants will be used (Table I: selected values). For the selected time constants, the computed temperature histories for 15K/min are shown in Figure 2 and the quality of the DTA fits is shown in Figure 3.

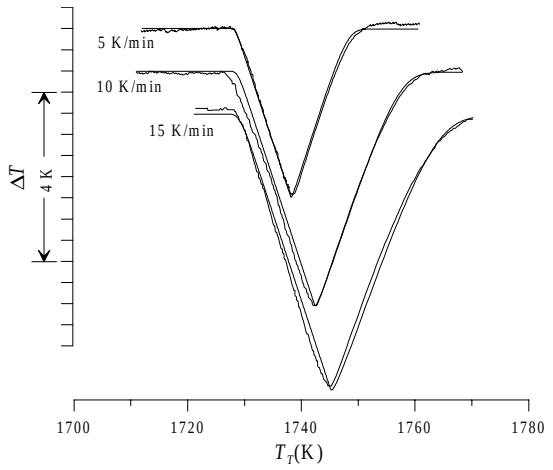

Fig. 3. Comparison of measured DTA curves ($\Delta T(T_T)=T_T-T_{ref}$) with calculated curves ($\Delta T(T_T)=T_T-T_W$) at heating rates of 5 K/min., 10 K/min. and 15 K/min. The noisy curve is the experimental data.

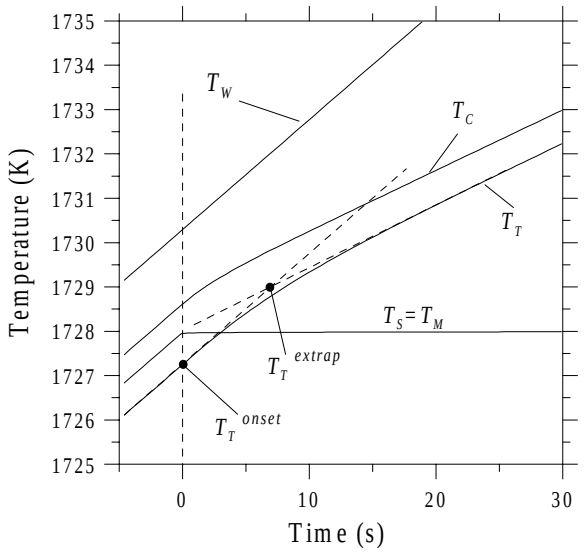

Fig. 4 Enlarged view of Fig. 2 near *t=0.*

D. Evaluation of Onset and Peak Temperatures and Peak Height of DTA Curve for Pure Material from Analytical Solution

We digress from the main topic of alloy DTA to indicate important features of the DTA plot for pure metals using the analytical results. The first is the onset of melting temperature measured by the thermocouple. Figure 4 shows an enlarged view of the temperature histories near the initiation of melting at t = 0. The onset temperature is the thermocouple temperature at $t = 0$ given by

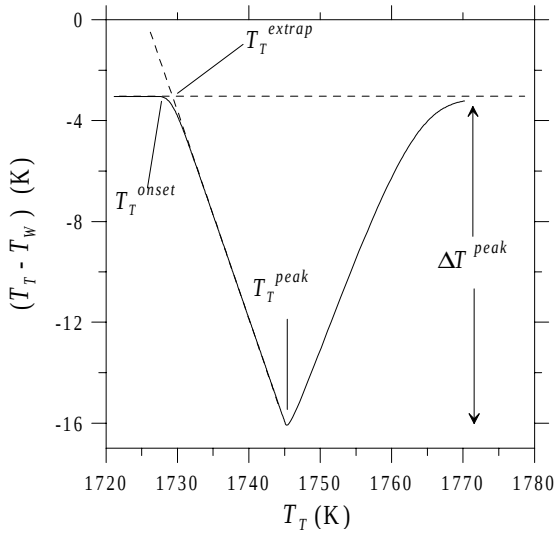

Fig. 5 Plot of calculated DTA curve, $\Delta T(T_T)$, corresponding to Fig. 2.

$$T_T^{onset} = T_T(0) = T_M + \alpha\,(t_{S,C}R - t_{T,C})\ , \qquad [12]$$

which for the values of the time constants given in Table I is 2.6 α (K if α is in K/s) below T_M or 0.6 K for a heating rate of 15 K/min. Figure 5 shows the calculated DTA signal corresponding to Figure 4.

Due to the trouble of picking the onset of the DTA signal graphically, either on a $T_T(t)$ plot or a $\Delta T(T_T)$ plot, an extrapolation procedure is commonly used to determine an alternate melting onset. This procedure takes advantage of the fact that the thermocouple temperature vs. time, $T_T(t)$, curve becomes linear quickly after the melting onset (Eq. [7], bottom). The asymptote[+] is given by

$$T_T^{asymp}(t) = T_M + \alpha\{t_{S,C}\,R - t_{T,C} + \frac{t_{W,C}\left[t_{S,C}t_{W,C} + t_{S,C}t_{T,C} + t_{W,C}t_{T,C}\right]}{(t_{S,C} + t_{W,C})^2}\ . \qquad [13]$$
$$+ \frac{t_{S,C}\,t}{t_{S,C} + t_{W,C}}\}$$

The alternate choice for the onset temperature is taken as the intersection of the asymptote and the baseline (the extrapolation forward of the DTA curve prior to melting). The intersection of the asymptote with the line for the extrapolated thermocouple temperature prior to melting, $T_T = T_M + \alpha\,(t + Rt_{S,C} - t_{T,C})$, occurs at time t^* given by

[+] The slope of the ΔT vs. T_T curve after onset is $-t_{W,C}/t_{S,C}$, which is independent of heating rate.

$$t^* = \frac{t_{S,C}t_{W,C} + t_{S,C}t_{T,C} + t_{W,C}t_{T,C}}{t_{S,C} + t_{W,C}} \quad . \qquad [14]$$

The melting onset picked in this way is given by

$$T_T^{extrap} = T_T^{asymp}(t^*) = T_M + \alpha\left(\frac{a(t_{S,C}R + t_{W,C}R + t_{W,C})}{t_{S,C} + t_{W,C}}\right) \qquad [15]$$

which is 5.2 α (K if α is in K/s) above T_M or 1.3 K at a heating rate of 15 K/min.

Until now we have assumed that the thermocouple is perfectly calibrated. In reality the thermocouple is usually calibrated using the melting signal itself using one of the two onset determination procedures. Then the offset from T_M in Eq. [12] or [15] is reduced to zero, but only for the heating rate of the calibration run. The DTA would require recalibration at each heating rate.

Another DTA detail of interest is the peak temperature. Clearly for a pure material it is far above the melting point and is given by Eq. [13] evaluated at t_M:

$$T_T(t_M) = T_M + \alpha[R t_{S,C} - t_{T,C} + \frac{t_{W,C}(t_{S,C}t_{W,C} + t_{S,C}t_{T,C} + t_{W,C}t_{T,C})}{(t_{S,C} + t_{W,C})^2} + \frac{t_{S,C}}{t_{S,C} + t_{W,C}}\alpha t_M \quad . \qquad [16]$$

Neglecting the small bracketed term and using the approximation (Eq.[10]) for t_M,

$$T_T^{peak} \approx T_M + \sqrt{\frac{2{t_{S,C}}^2 m_S L\alpha}{m_C C_p^C (t_{S,C} + t_{W,C})}} \quad . \qquad [17]$$

For the parameters in Table I, the peak temperature is 17.1 K above T_M for 15 K/min

The DTA peak height below the baseline is another parameter of interest. It is given by

$$\Delta T(t_M) - \Delta T(0) = \alpha\left[\frac{t_{W,C}(t_{S,C}t_{W,C} + t_{S,C}t_{T,C} + t_{W,C}t_{T,C})}{(t_{S,C} + t_{W,C})^2}\right] - \left(\frac{\alpha t_{W,C}t_M}{t_{S,C} + t_{W,C}}\right) \quad . \qquad [18]$$

Again, neglecting the small bracketed term and using the approximation for t_M,

$$\Delta T(t_M) - \Delta T(0) \approx -\sqrt{\frac{2m_S L\alpha {t_{W,C}}^2}{m_C C_p^C (t_{S,C} + t_{W,C})}} \quad . \qquad [19]$$

For the parameters in Table I the peak height is 14.7 K for 15 K/min. Note that while reducing α decreases the difference between the onset and peak, it also decreases the peak height. This is the usual compromise that must be reached with DTA measurements between accuracy and sensitivity.

The peak "area" is often used to measure the heat of reaction, in this case the heat of fusion. The peak area can be obtained either from the $\Delta T(t)$ curve or the $\Delta T(T)$ curve with corresponding units of K·s or K^2, respectively. For the former, the area is

$$A^{peak} = \int_0^\infty [\Delta T(t) - \Delta T(0)]dt \quad . \qquad [20]$$

The evaluation of this integral for the analytical solution is complex. Numerical evaluation showed A^{peak} to be proportional to the product of sample mass and latent heat as expected. We note that the product of the approximate forms for the peak height and the difference between the peak position and the melting point is also proportional to the product of sample mass and latent heat.

IV. DTA Melting Signals for Alloys

A. The effect of freezing range on the measurement of liquidus

If we take a simple binary temperature vs. composition phase diagram with straight line liquidus and solidus curves

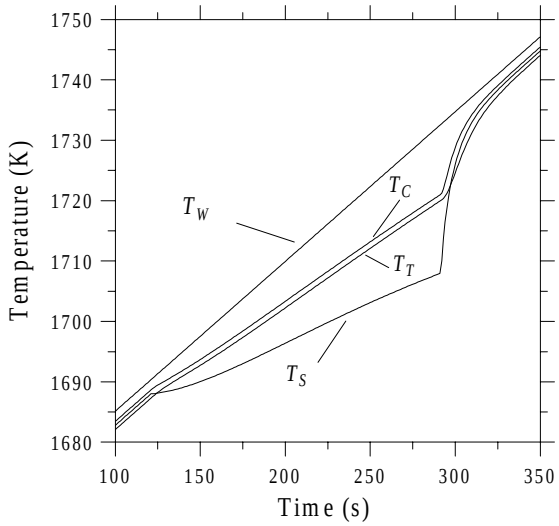

Fig. 6 Plot of calculated sample, sample cup, sample thermocouple and furnace wall temperatures vs. time for melting at a heating rate of 15 K/min of a 180 mg binary alloy sample that melts following the lever rule. T_M=1728 K, m= -10^3 K/mass fraction, k=0.5, C_0=0.02 mass fraction.

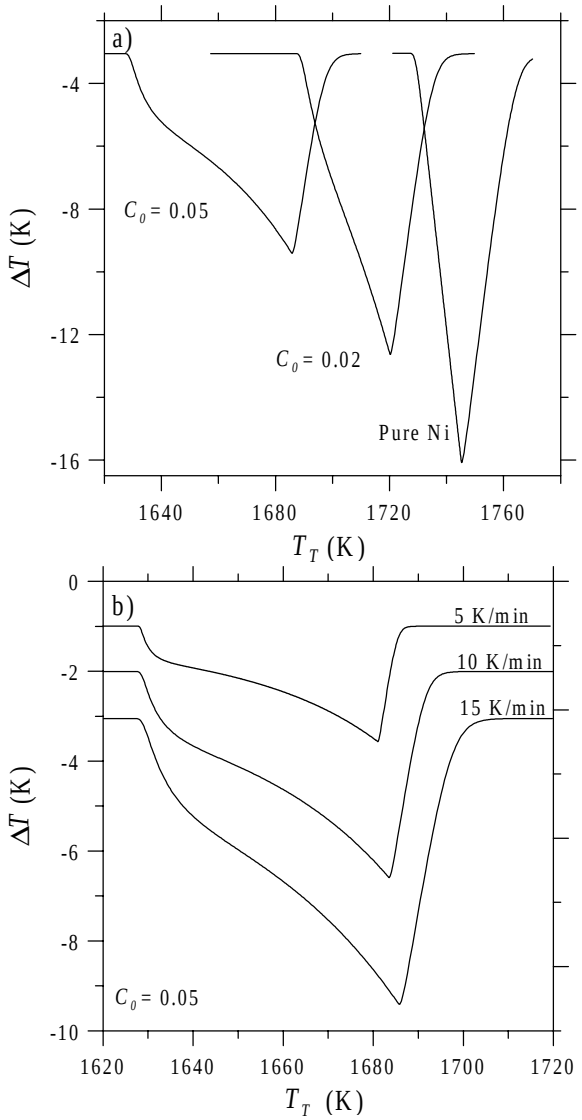

Fig. 7. a) Calculated DTA curves for pure Ni and alloys with C_0 = 0.02 and 0.05 mass fraction following the lever rule at 15 K/min.
b) Calculated DTA curves for alloy with C_0 = 0.05 mass fraction following the lever rule at heating rates of 5, 10 and 15 K/min.

$$\begin{aligned} T_{Liq} &= T_M + m\,C_0 \\ T_{Sol} &= T_M + (m/k)C_0 \end{aligned} \qquad [21]$$

with concentration C_0, liquidus slope m and partition coefficient k, the enthalpy-temperature for an equilibrium liquid - solid mixture (lever law) is given by

$$H_S(T_S) = C_p^{S0} T_S + L\left[1 + \left((1-k)\left(\frac{T_S - T_{Sol}}{T_{Liq} - T_S}\right)\right)^{-1}\right] . \qquad [22]$$

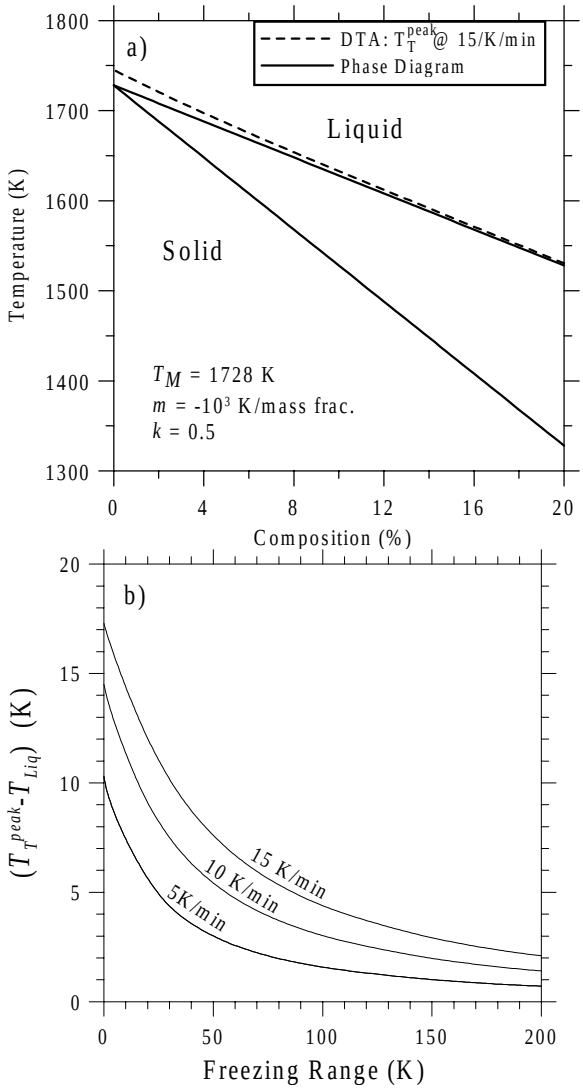

Fig. 8. a) DTA peak temperature calculated at a heating rate of 15 K/min for different alloy compositions using a lever assumption. Peak temperature is superimposed on the phase diagram (T_M=1728 K, m= -10^3 K/mass fraction, k=0.5).
b) The difference between the peak temperature and the liquidus temperature as a function of freezing range at three heating rates. The freezing range is given by $m_L C_0[(k-1)/k)$.

For a heat capacity $H'_S(T_S)$ for all temperatures defined as

$$H'_S(T_S) = \begin{cases} H'(T_S) & \text{if} \quad T_{Sol} < T_S < T_{Liq} \\ C_p^{S0} & \text{otherwise} \end{cases} \qquad [23]$$

the numerical solution of Eq. [1] yields the temperature - time histories given in Figure 6. As for the case of the pure material, various onsets can be defined that all differ from the exact solidus temperature. Here we focus however on the liquidus temperature.

It is often difficult to measure the liquidus temperature during freezing because of supercooling (especially with Ni alloys). Melting data is often preferred to determine the liquidus. It is therefore important to note the behavior of the DTA signal as the sample completes melting. At this time, the thermocouple temperature is higher than the liquidus temperature. The simulated DTA signals at 15 K/min for hypothetical Ni-based alloys are shown in Figure 7(a). The phase diagram is given by T_M=1728 K, m = -10^3 K/mass frac. and k=0.5 and the compositions are C_0 = 0 .0 mass fraction (pure Ni), 0.02 mass fraction, 0.05 mass fraction. Figure 7(b) shows the effect of heating rate for C_0 = 0.05. The peaktemperature as a function of alloy composition for 15 K/min is shown superimposed on the phase diagram in Figure 8(a). The difference between the peak and the liquidus temperatures is shown in Figure 8(b) for different heating rates. The error increases as the size of the freezing range decreases. For large freezing range alloys, the latent heat evolution is spread over a large temperature range and the offset between the sample temperature and the sample thermocouple temperature is small. But for alloys with small freezing ranges, care must be taken in attempting to determine the liquidus temperature from the melting peak. The error is exacerbated by inclusion of the melting kinetics described in Section V - A.

B. Melting of Multicomponent Alloys

We now explore the DTA melting response of a pair of complex alloys. As input to the calculation we use enthalpy vs. temperature values obtained for full equilibrium (lever law) and for Scheil freezing assumptions. DTA melting simulations, using the lever enthalpy-temperature relation, would apply to an alloy equilibrated prior to melting and where diffusion was adequate to guarantee spatial concentration uniformity of all phases during melting. DTA melting simulations, using the Scheil enthalpy calculations, would apply to a microstructure that was solidified *and* remelted with no solid diffusion. Clearly these are extreme cases. The melting of an equilibrated alloy as well as an as-cast sample requires an analysis of solid diffusion for both the freezing process and the melting process. For the lever and Scheil cases, the thermodynamic parameters of Saunders[23,24] were used in conjunction with the methods of Boettinger et al.[25] to give the enthalpy - temperature relations.

Table II. Sequence of phase formation during lever and Scheil freezing of 2219 Al Alloy

Lever	Scheil
$L \leftrightarrow$ fcc	$L \rightarrow$ fcc
$L \leftrightarrow$ fcc + Al_6Mn	$L \rightarrow$ fcc + Al_6Mn
$L + Al_6Mn \leftrightarrow$ fcc + Al_7Cu_2Fe	$L \rightarrow$ fcc + Al_7Cu_2Fe
	$L \rightarrow$ fcc + Al_7Cu_2Fe+Al_2Cu
$L \leftrightarrow$ fcc + Al_7Cu_2Fe	$L \rightarrow$ fcc + Al_7Cu_2Fe+Al_2Cu+α-AlFeSi
$L \leftrightarrow$ fcc + Al_7Cu_2Fe + $Al_{20}Cu_2Mn_3$	
$L \leftrightarrow$ fcc + Al_7Cu_2Fe + $Al_{20}Cu_2Mn_3$ + Al_2Cu	$L \rightarrow$ fcc + Al_7Cu_2Fe + Al_2Cu + α-AlFeSi + Si (Invariant reaction at 797K)

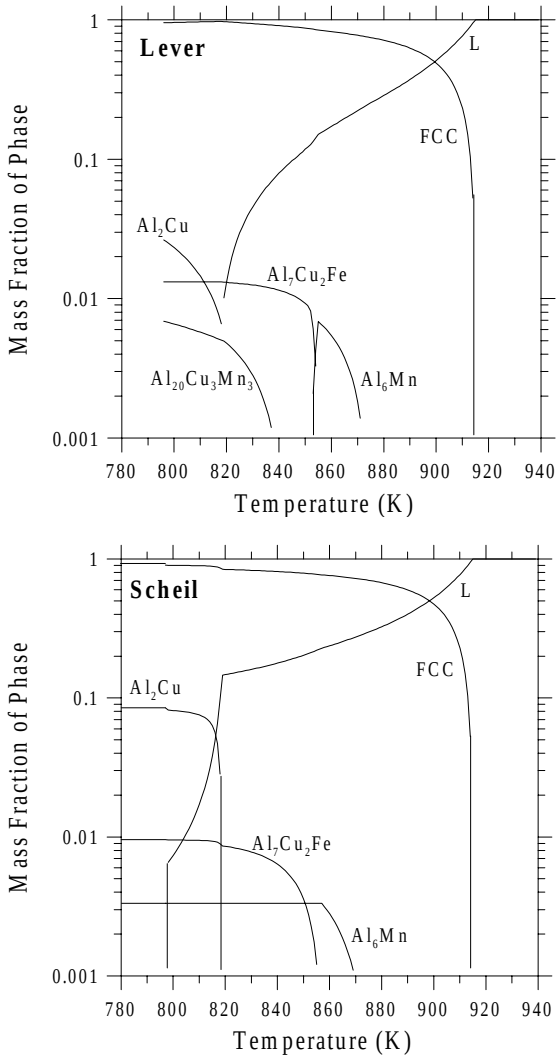

Fig. 9. Phase fraction vs. temperature computed using thermodynamic database [23] for lever and Scheil conditions for Al 2219 alloy.

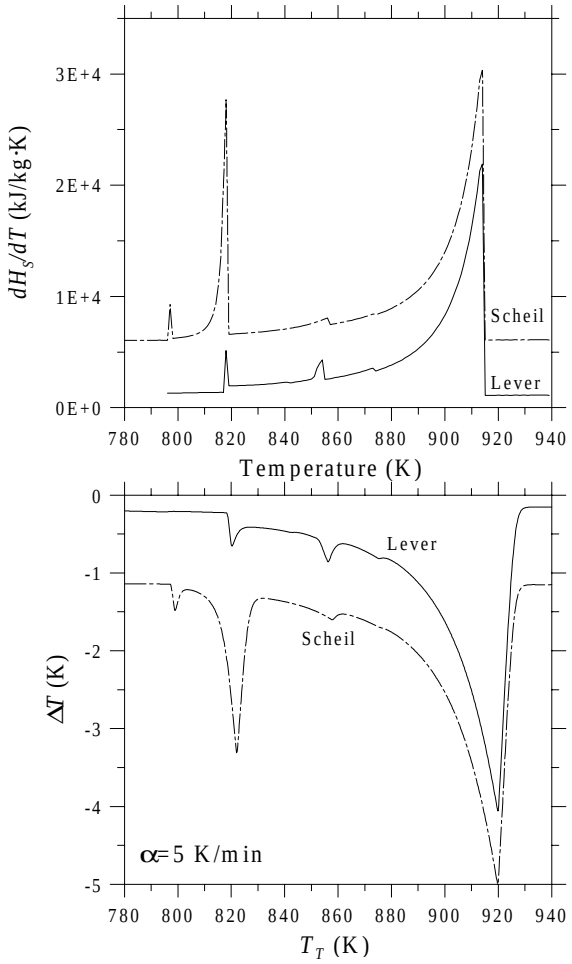

Fig. 10. Top) dH_S/dT obtained from the enthalpy - temperature predictions for Al 2219 alloy computed using thermodynamic database [23] for lever and Scheil conditions for Al 2219 alloy. The curve for 'Scheil' is shifted up by $5x10^3$ kJ/kg K for clarity.
Bottom) Corresponding DTA plots for melting at 5 K/min.. The curve for 'Lever' is shifted up 1 K for clarity.

1. Example: Al 2219

Al alloy 2219 has typical mass fractions of 0.0663 Cu, 0.003 Mn, 0.002 Fe and 0.001 Si. Table II gives the sequence of phase formation 'reactions' listed in the order of decreasing temperature. More phases occur, and the final solidification temperature is lower for the Scheil assumption due to the microsegregation in the primary fcc phase. Figure 9 shows the phase fractions as a function of temperature. Off of the scale of Figure 9 are the α-AlSiFe and Si phases with maximum phase fractions of 8×10^{-4} and 3×10^{-4} respectively.

Figure 10 shows the values of dH_S/dT obtained from the calculated enthalpy temperature - curves and the DTA simulation for 5 K/min. Comparison of

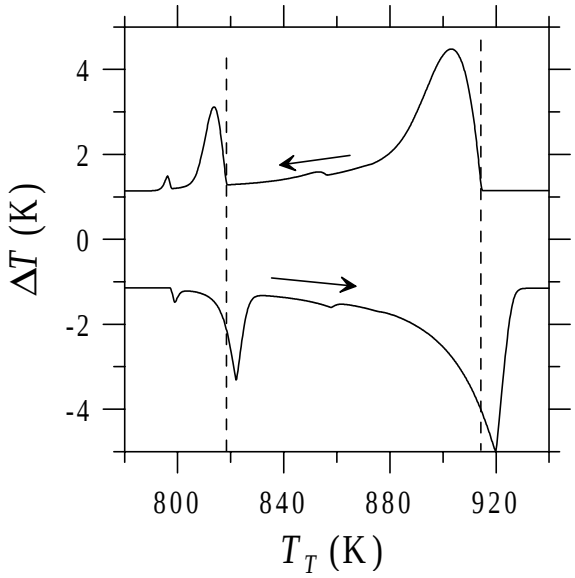

Fig. 11. Calculated DTA plots for melting and freezing at 5 K/min of Al 2219 alloy using the Scheil enthalpy-temperature relation.

Figure 9 with the dH_S/dT curves allows one to recognize the cause of the various peaks in the DTA signal. During melting, a peak occurs when all of a particular phase has completely melted. For example for the lever melting, the first peak on heating indicates that all of the Al_2Cu phase has melted. The second peak indicates that all of Al_7Cu_2Fe has melted and similarly for other peaks. Note that for the Scheil DTA calculation, a peak is visible at approx. 797 K. This is due to the melting of the invariant quinary eutectic at 797K (Table II) where the Si phase completely disappears and importantly reductions also occur in the phase fractions of the other phases. The alloy under consideration has five components, the reaction involves six phases, and there are zero degrees of freedom. Thus despite the small fraction of Si phase, the signal from the invariant eutectic melting is large. We note that the DTA time constants, should be re-assessed using melting of a pure metal whose melting point is closer to that of Al for future quantitative comparisons to experiment.

Simulations of alloy freezing were performed by changing the sign of α and the values of the start temperatures. Figure 11 compares the melting and freezing signals for the Al 2219 alloy at 5 K/min (Scheil enthalpy used for both). The vertical dashed lines are the liquidus temperature and the temperature where the Al_2Cu phase disappears, or first appears, on melting or solidification, respectively. The peak temperatures are clearly offset from these dashed lines and should not used to characterize the melting or freezing process.

2. UDIMET 700

A second example is the Ni alloy, UDIMET† 700, with composition in mass fractions of 0.15 Cr, 0.185 Co, 0.05 Mo, 0.035 Ti, 0.044 Al, 0.0007 C, and 0.00025 B. The thermodynamic parameters were taken from Saunders[24]. The phase formation sequences are given in Table III, the phase fractions in Figure 12 and dH_S/dT and the DTA signals in Figure 13. To be noted here is the very large difference between the size of the freezing ranges of the two cases. The particular peaks and their sizes for real DTA signals for this alloy would be difficult to predict given the large difference between the diffusion rates of the interstitials and the substitutional elements in the fcc phase.

Table III - Sequence of phase formation during lever and Scheil freezing of UDIMET 700

Lever	Scheil
L	$L \rightarrow fcc$
L + fcc	$L \rightarrow fcc + MC$
L + fcc + MC	$L \rightarrow fcc + MC + MB_2$
L + fcc + MC + MB_2	$L \rightarrow fcc + MC + M_3B_2$
	$L \rightarrow fcc + MC + M_3B_2 + \sigma$
	$L \rightarrow fcc + MC + M_3B_2 + \sigma + \gamma'$
fcc + MC + MB_2	$L \rightarrow fcc + MC + \sigma + \gamma' + MB_2$

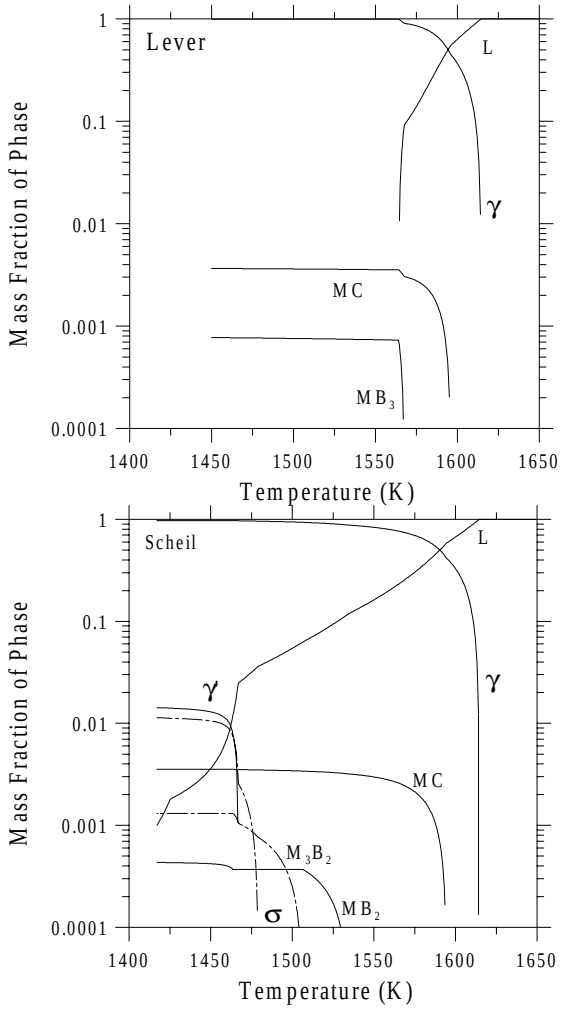

Fig. 12 Phase fraction vs. temperature computed using thermodynamic database [24] for lever and Scheil conditions for UDIMET 700 alloy.

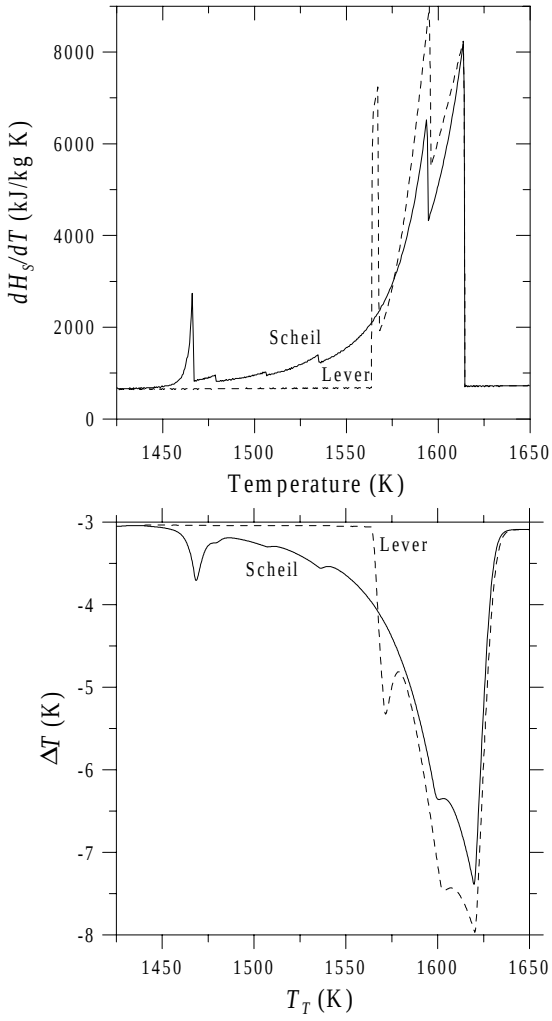

Fig. 13. Top) dH_S/dT obtained from the enthalpy - temperature predictions for Udimet 700 alloy computed using thermodynamic database [24] for lever and Scheil conditions for Udimet 700 alloy.
Bottom) Corresponding DTA plots for melting of 180 mg sample at 15 K/min

† UDIMET is a trademark of Special Metals Corporation, New Hartford, NY.

One can now recognize possible confusion that occurs on the interpretation of DTA for complex alloys. Real DTA traces would likely lie somewhere between the Lever and Scheil cases depending on many factors. What is the state of the alloy when melting begins? Has it been solidified by a prior DTA run? What was the segregation produced by that run? How long has it been held in the solid state prior to the initiation of the next melting run? How much diffusion occurs during the melting process? Is there enough time to ensure spatial uniformity of all components in each phase?

V. Inclusion of Kinetics in DTA Response

A. Melting

Until now, the enthalpy of the sample for the melting process has been a specified function of temperature. In reality the speed of solute diffusion can alter the enthalpy evolution of the sample. As a first step to treat diffusion, a model can be constructed along the lines presented by Basak et al.[26] for melting of a single phase solid. The time rate of change of the enthalpy of the sample (Eq. [4]) is replaced by

$$\dot{H}_S = \frac{dH_S}{dt} = C_p^{S0}\dot{T}_S - L\dot{f}_S \,, \qquad [24]$$

where $f_s(t)$ is the fraction solid. This expression provides the coupling between the DTA heat flow equations and the kinetic micromodel. Assumptions about the melting geometry and a consideration of diffusion equations are required to describe the temperature and the fraction of solid at each instant during the melting process.

In Figure 14, we consider of a 1-D solid slab of initial uniform composition C_0 with melting beginning at one side and proceeding to the other (or a cylindrical or spherical region where melting begins at the outside and proceeds inward). We further assume that the liquid concentration is uniform and given by $C_L(t)$ and that the solid concentration $C_S(r,t)$, although initially uniform, varies with time and position, r, during the melting process. The melting interface is located at $r_0(t)$ and changes from a value of R_M (all solid) to 0 (all liquid) as melting progresses; i.e., $2R_M$ is a measure of the distance between adjacent liquid regions within the sample.

A value for R_M can only be estimated. Melting usually starts at grain boundaries in a homogenized sample, R_M would be the grain size radius and a spherical geometry would be appropriate. If the sample were a single grain, then R_M would equal the sample radius, 1.5 mm for a 180 mg sample of Ni.

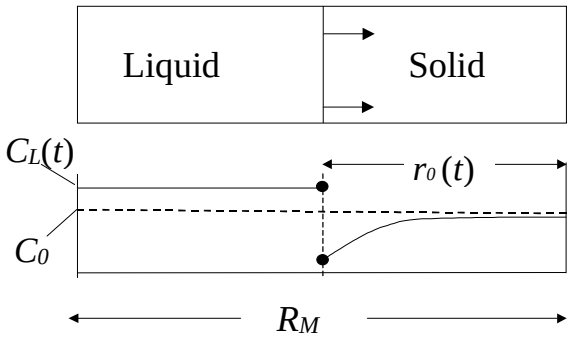

Fig. 14. Diffusion geometry analyzed during melting. Slab geometry (n=1) is shown.

This can serve as an upper bound on R_M. If some slight residual dendritic coring is present in the *homogenized* sample, a much smaller value would be appropriate; viz., the dendrite arm spacing from previous solidification of the sample (~150 μm).

Assuming local equilibrium at the melting interface and ignoring the Gibbs-Thomson effect, the temperature of the interface (and hence the sample temperature, $T_S(t)$) is related to the (uniform) liquid concentration by

$$T_S(t) = T_M + m\,C_L(t) \quad . \qquad [25]$$

The solid concentration at the interface is related to the liquid concentration (at the interface) by

$$C_S(r_0(t),t) = kC_L(t) \quad . \qquad [26]$$

On the interval [0, $r_0(t)$], the solid concentration profile is governed by the solid diffusion equation

$$\frac{\partial C_S}{\partial t} = D_S\nabla^2 C_S = \frac{D_S}{r^{n-1}}\frac{\partial}{\partial r}\left[r^{n-1}\frac{\partial C_S}{\partial r}\right] \,, \qquad [27]$$

where D_S is the solid diffusion coefficient and the geometrical factor, n, is equal to 1, 2, 3 denoting a slab, cylinder or sphere respectively. The initial condition is $C_S(r,0)=C_0$ and a no flux condition is applied at $r=0$. The boundary condition at $r=r_0(t)$ is obtained by considering a solute balance at any time during melting over the entire domain [0, R_M]; viz.,

$$\frac{n}{R_M{}^n}\int_o^{r_0(t)} C_S(r,t)r^{n-1}dr + C_L(t)(1-f_S) = C_0 \qquad [28]$$

with the fraction solid, $f_S(t) = [r_0(t)/R_M]^n$. Differentiation of Eq. [28] with respect to t and substituting Eq. [27] to eliminate $\partial C_S/\partial t$ yields the boundary condition at the melting interface ($r=r_0(t)$) given by

$$n f_S^{(n-1)/n} \frac{D_S}{R_M} \left.\frac{\partial C_S}{\partial r}\right|_{r=r_o(t)} + (k-1)\dot{f}_S C_L + (1-f_S)\dot{C}_L = 0 \ . \quad [29]$$

In the spirit of using only ordinary differential equations in this paper, an approximate solution to the solute diffusion equation can be obtained. Along lines similar to those of Wang and Beckermann[27] for freezing, the solute profile in the solid is assumed to be a polynomial in r with time dependent coefficients of the form $a(t)+b(t)r^p$. For a solute profile that satisfies the no flux condition at $r=0$ and Eqs.[260 and [28], the gradient term in Eq. [29] can be evaluated as

$$\left.\frac{\partial C_S}{\partial r}\right|_{r=r_o(t)} = -\frac{(n+p)}{R_M}\left[\frac{C_0 - [1-f_S(1-k)]C_L}{f_S^{(n+1)/n}}\right] . \quad [30]$$

Equation [29] then becomes an ODE for $f_S(t)$ and $C_L(t)$. Combining this ODE and Eq. [25] in differential form to the three DTA heat flow equations, one obtains:

$$\begin{cases} m_S\left[C_p^{S0}\dot{T}_S - L\dot{f}_S\right] = \dfrac{m_C C_C}{t_{S,C}}(T_C - T_S) \\ \dot{T}_C = \dfrac{1}{t_{S,C}}(T_S - T_C) + \dfrac{1}{t_{W,C}}(T_W - T_C) \\ \dot{T}_T = \dfrac{1}{t_{T,C}}(T_C - T_{TC}) \\ \dot{T}_S = m_L \dot{C}_L \\ (k-1) f_S C_L + (1-f_S)\dot{C}_L = \\ \qquad n(n+p)\dfrac{D_S}{R_M{}^2}\left\{\dfrac{C_0 - [1-f_S(1-k)]C_L}{f_S^{2/n}}\right\} \end{cases} . \quad [31]$$

The equations are ill-posed at $t=0$ ($f_S = 1$), and only a small error is introduced by using the following conditions at the beginning of melting,

$$\begin{aligned} f_S(0) &= 1-\varepsilon \\ C_L(0) &= C_0/[1-\varepsilon\,(1-k)] \end{aligned} , \quad [32]$$

where $\varepsilon << 1$

The equations involve the important ratio, $D_S/R_M{}^2$. In dimensionless form, a solid diffusion Fourier number, $F_o = D_S t_M{}^{alloy}/R_M{}^2$, can be defined where $t_M{}^{alloy}$ is the alloy melting time

$$t_M^{alloy} \approx \sqrt{\frac{2m_S(L + C_p^S(T_L - T_S))(t_{S,C} + t_{W,C})}{\alpha\, m_C C_p^C}} \quad [33]$$

determined in analogy with Eq. [10]. The coefficient D_S at the solidus temperature of a substitutional solid solution is at most 10^{-8} cm^2/s and $t_M{}^{alloy} \approx$ 500s, 400,

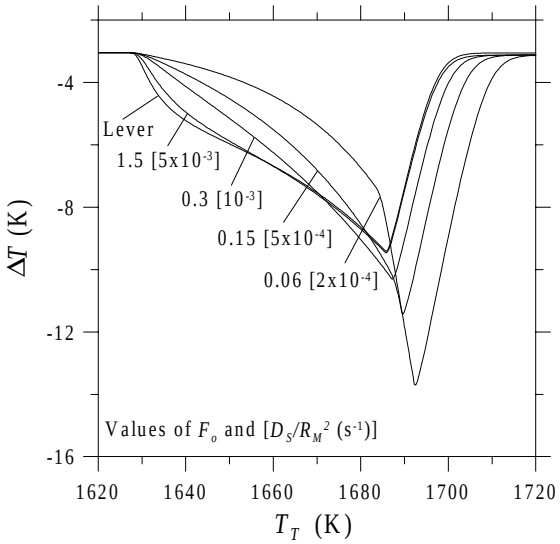

Fig. 15. Effect of solid diffusion on melting DTA signal of single phase alloy, n=3, α=15 K/min., T_M=1728 K, m= -10^3 K/mass fraction, k=0.5, C_0=0.05 mass fraction. Results for various values of the Fourier Number, F_o, and $D_S/R_M{}^2$ are shown.

300 s (for a 180 mg Ni alloy sample with a 50 K freezing range heated at 5, 10 and 15 K/min, respectively). Using the values for R_M discussed above, $4\text{x}10^{-7}$ s^{-1} $<D_S/R_M{}^2<4\text{x}10^{-3}$ s^{-1}, and the Fourier Number for $t_M{}^{alloy}=300$ s lies in the range, $1\text{x}10^{-4}<F_o<1$.

We show results for an alloy with T_M=1728 K, m= -10^3 K/mass fraction, k=0.5 and C_0=0.05 mass fraction, the spherical geometry ($n=3$) and $p=3$. The results are not very sensitive to the value of p. The calculated DTA signal for F_o= 10 (plenty of diffusion) is indistinguishable from that for melting following the lever law and is not shown. This agreement provided a good check on the calculation procedure. The DTA signals shown in Figure15 exhibit three changes as the F_o decreases: 1) the change in slope at the solidus becomes smaller; 2) the peak shifts to higher temperatures; and 3) the peak height increases. These changes are caused by the fact that solid diffusion limitations cause a larger fraction of the solid to melt at temperatures closer to the liquidus compared to what occurs when the solid composition remains spatially uniform. Thus it is harder to establish an onset of melting. At the end of melting, a larger temperature offset occurs between the sample temperature and the sample thermocouple temperature than would occur for melting with a lever enthalpy. Thus the peak temperature becomes even more unreliable as a measure of the liquidus temperature when diffusion limitations are present. Table IV summarizes the effect of solid diffusion on

Table IV - Effect of Solid Diffusion Limitation During Melting on "Liquidus" DTA Peak

D_S/R_M^2 (s^{-1})	F_o (t_M^{alloy}=300 s)	T_T^{peak}-T_L (K)	ΔT^{peak} (K)
∞ (lever)	∞	8.1	6.3
$5x10^{-3}$	1.5	7.9	6.4
$1x10^{-3}$	0.3	9.2	7.2
$5x10^{-4}$	0.15	11.7	8.4
$2x10^{-4}$	0.06	14.4	10.7
0 (as a pure material w/T_M=T_L)	0	17.6	16.1

α= 15 K/min, C_0=0.05 mass fraction, k=0.5, m= -10^3 K/mass fraction, T_M=1728 K (T_{Liq}=1678 K. T_{Sol}=1628 K).

the liquidus peak temperature for a 180 mg Ni alloy with a 50 K freezing range alloy melted at 15 K/min.

During the numerical calculations for $F_o < 0.2$, the approximation of Eq. [30] leads to liquid compositions lower than C_0 during melting. This is not possible for a binary alloy and is an artifact of the approximate solution to the diffusion equation. In such cases, the diffusion calculation was truncated at the time when the liquid composition decreases to C_0. The DTA temperatures after that time are computed assuming the sample temperature remains at the liquidus temperature until the fraction solid reaches zero. With this procedure, the DTA curve at the higher temperatures approaches that for melting of a pure metal with a melting point equal to the alloy liquidus temperature. This would also happen in a rigorous calculation of the diffusion process as F_o becomes very small. While this limiting situation is unlikely physically, it demonstrates the worst case for solid diffusion restrictions during melting.

Thus if a substitutional alloy sample is homogenized and consists of only a few grains ($F_o < 10^{-3}$), the diffusion limitation should make a considerable change in the shape of the DTA curve. Only rarely would the observed DTA curve resemble that for lever melting. Residual microsegregation from prior solidification might reduce the length scale R_M, increase the value of F_o, and reduce the peak error, but it would also lower the melting onset temperature below the true solidus. A fast diffusion mechanism could also mitigate the calculated effect of diffusion restrictions during melting. One possible fast mechanism might be liquid film migration during melting. Nonetheless, because the freezing range of the alloy simulated (50 K) is not unlike the commercial alloys studied by Wu and Perepezko[18], the present melting model may provide an explanation for their observation that the DTA peak temperature was 20 K higher on melting at 20 K/min than the actual liquidus temperature. This is especially so given the slow diffusion of the refractory elements in superalloys. We note that for an interstitial binary alloy, F_o would be about 2 orders of magnitude larger.

B. Inclusion of Dendrite Tip Kinetics (Supercooling) in DTA Response During Freezing

A common occurrence in DTA analysis during cooling from the fully molten state is supercooling. In Ni base alloys, supercoolings as large as 100 K are common before nucleation of the solid phase. The DTA response to this situation can be modeled from a knowledge of the nucleation temperature, T_N, the number of nuclei (or final grain size) and the kinetics of the growing solid. Often in supercooled samples in the DTA, only one grain is formed.

Here we briefly describe a model for the kinetics of a binary alloy freezing in a dendritic manner. The approach of Wang and Beckermann[27] is employed and the reader is referred to this work for a more complete discussion of the model. To the three equations for the DTA response, we append five ODE's that describe the liquidus slope, the dendritic growth kinetics, the liquid diffusion, the solid diffusion and an overall solute balance. The five equations involve the five variables $f_g(t)$, $f_s(t)$, $C_L(t)$, $<C_L>(t)$ and $<C_S>(t)$ for the fraction of grain, the fraction solid, the liquid concentration in the mushy region of the grain, the average liquid concentration outside of the mushy region (extradendritic liquid) and the average solid concentration, respectively. The fraction of grain variable is fraction of the final grain volume (sphere of radius R_g) that is occupied by the growing dendrite envelope at each instant. For this simple model, the speed of the dendrite tips is taken to depend on the square of the tip supercooling. The supercooling is taken as the difference between the tip temperature (i.e., sample temperature) and the liquidus temperature for the average liquid concentration outside of the mushy region. The liquid concentrations are governed by the solute rejection within the mush and by the solute diffusing into the extradendritic envelope. Diffusion in the solid is modeled with an equation that describes this average solid composition at each instant and estimates the solid concentration gradient in much the same way as in equations during melting (Eqs. [27] through [29]). Combining these five equations with the three for the heat flow in the DTA gives a system of eight ODE's for eight variables,

Table V - Parameters used for dendritic growth DTA simulations

Γ	D_L	m	k	C_0	T_M	L	C_p^{S0}	R_g	$m_C C_p^C$	m_S	D_S
10^{-5} cmK	10^{-5} cm^2/s	-10^3 K/mass fraction	0.5	0.05 mass fraction	1728 K	290 J/g	0.75 J/g K	1.5 mm	0.257 J/K	180 mg	0 cm^2/s

$$
\begin{cases}
m_S\left[C_p^{S0}\dot{T}_S - L\dot{f}_S\right] = \dfrac{m_C C_p^C}{t_{S,C}}(T_C - T_S) \\
\dot{T}_C = \dfrac{1}{t_{S,C}}(T_S - T_C) + \dfrac{1}{t_{W,C}}(T_W - T_C) \\
\dot{T}_T = \dfrac{1}{t_{T,C}}(T_C - T_{TC}) \\
\dot{T}_S = m\dot{C}_L \\
\dot{f}_g = \dfrac{3 f_g^{2/3}}{R_g}\ \dfrac{m_L D_L}{\pi^2 \Gamma (k-1) C_L}\left[C_L - < C_L >\right]^2 \\
(k-1)\dot{f}_S C_L + (f_g - f_S)\dot{C}_L = -\dfrac{\dot{f}_g}{(1-f_g)}\left[C_L - < C_L >\right] \\
(1-f_g) < \dot{C}_L > + \dot{f}_g C_L - \dot{f}_g < C_L > = \dfrac{\dot{f}_g}{(1-f_g)}\left[C_L - < C_L >\right] \\
\dot{f}_S < C_S > + f_S < \dot{C}_S > = k C_L \dot{f}_S + \dfrac{12 D_S}{\lambda_2}\dfrac{f_g\left[k C_L - < C_S >\right]}{f_S}
\end{cases}
\qquad [34]
$$

The parameter Γ is the ratio of liquid-solid surface energy per unit volume to the heat of fusion L. The parameter λ_2 is the secondary dendrite arm spacing. An important quantity in the Wang-Beckerman[27] approach is the extradendritic diffusion length, l_{id} (their symbol). For simplicity, rather than use their expression, we have let

$$l_{id} = \frac{D_L}{V}(1 - f_g) \quad , \qquad [35]$$

where V is the dendrite tip speed. The factor $(1\text{-}f_g)$ is used to reduce the diffusion length when little extradendritc liquid remains. These equations are solved with the initial conditions

$$
\begin{aligned}
T_S(0) &= T_N \\
C_L(0) &= (T_N - T_M)/m \\
f_S(0) &= 0 \\
f_g(0) &= 0
\end{aligned}
\quad . \qquad [36]
$$

The solution to these equations was obtained for the parameters specified in Table V. Solid diffusion was neglected and R_g was taken to be the sample radius; i.e., only one grain formed.

The initial parts of the sample, cup, thermocouple and wall temperatures histories are shown in Figure 16(a) for an initial supercooling of 0 K. Also shown

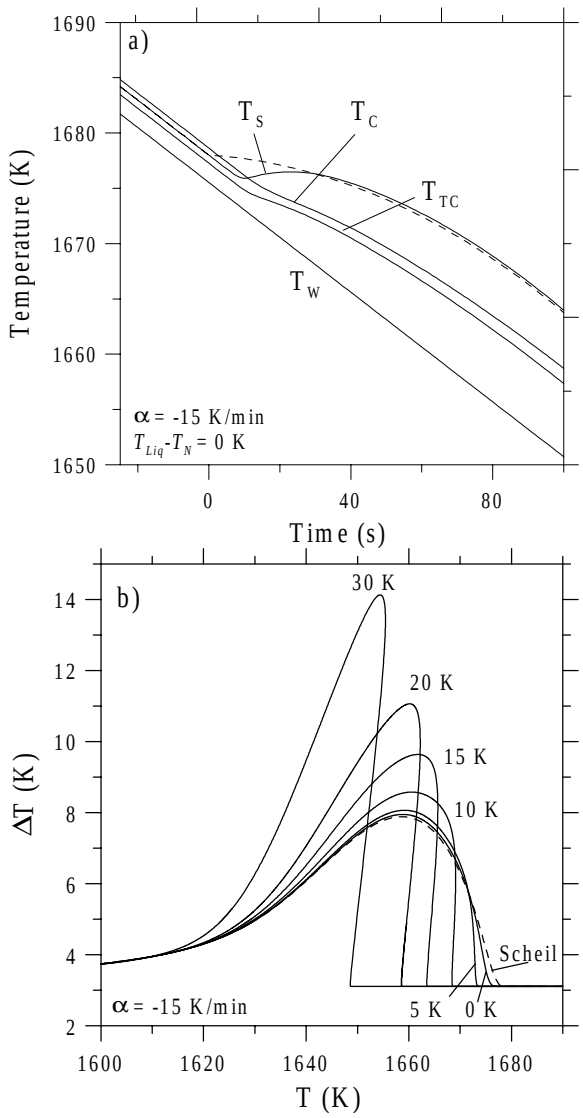

Figure 16. a) Plot of calculated sample, sample cup, sample thermocouple and furnace wall temperatures vs. time curves for freezing of a 180 mg sample of alloy with C_0 = 0.05 at 15 K/min with a supercooling of 20 K. b) Effect of supercooling on the freezing DTA signal of the same alloy. The curves are for 0 K, 5 K, 10 K, 15 K, 20 K, 30 K supercooling.

is the sample temperature (dashed curve) for a DTA calculation performed using a Scheil solidification path for the same alloy. Several feature can be noted: 1) Even for the case of zero supercooling, a slight recalescence of the sample temperature occurs due to the finite speed at which the dendrites can propagate across the sample; 2) After the recalescence, the sample temperature converges to the sample temperature calculated for the Scheil path. This agreement provided a good check on the computational approach. 3) The cup and thermocouple temperatures exhibit no recalescence due to the heat transfer restrictions of the DTA cell.

The initial portions of DTA curves for initial supercoolings of 0 K, 5 K, 10 K, 15 K, 20 K and 30 K are shown in Figure 16(b) along with the DTA curve for the Scheil path. The initial rise of the DTA signal departs the baseline at lower temperatures and rises more rapidly as the supercooling increases. This is due the recalescence of the sample due to the rapid initial dendritic growth. The rise has a backward (positive) slope only for supercoolings of 10 K and above. Here the sample recalescence is large enough that the thermocouple temperature also recalesceces. However, the absence of a backward DTA rise is not proof that supercooling is absent and that a valid liquidus temperature has been determined.

VI. Conclusions and Future Work

DTA is widely used for the measurement of alloy solidification and melting behavior. This study indicates the care that must be taken in order to extract meaningful data from experiments. A heat flow model combined with kinetic models appropriate for metallic systems is used to simulate DTA data during melting and freezing. An analytical solution of the model for a pure material is used to show how the melting onset and peak temperatures depend on sample mass and heating rate and thus how they affect calibration procedures. In particular, sample and sample thermocouple temperatures in the DTA instrument can exhibit large differences that are often forgotten in the interpretation of DTA signals. Numerical solutions of the heat flow model employing enthalpies obtained from a Calphad-type thermodynamic assessments are used to simulate DTA signals for a two multicomponent engineering alloys. The simulations show the differences between thermodynamic points and features on the DTA curve caused by heat flow limitations in the DTA. As such the method provides a tool to enable a more reliable interpretation of signals from unknown materials. [The MATHEMATICA script will be made available at www.metallurgy.nist.gov/phase/].

In addition to heat flow effects, the DTA signal is influenced by diffusion kinetics within melting and freezing samples. A methodology for including kinetics into the simulation of DTA signals is established. For melting, the simulations show that the use of the temperature of the final peak in the DTA curve is of limited validity to determine the liquidus temperature of alloys with small freezing ranges (<50K) and with sluggish solid diffusion. For freezing, the simulations show the quantitative relationship between supercooling and the shape of the DTA curve.

Future work should include a detailed comparison of the predictions of the diffusion based melting model to experimental data and extension of the model to multicomponent alloys. The appropriate diffusion length scale, whether it be grain size or residual microsegregation length, needs to be studied. Deconvolution methods based on realistic melting and solidification models should be developed to extract reliable solidification information from DTA signals.

Acknowledgement

The authors would like to express their appreciation to N. Saunders for the use of the thermodynamic data bases for Al and Ni alloys. Also thanks are in order to D.K. Banerjee for early work on this subject and to J.H. Perepezko for stimulating the authors' interest in DTA.

Appendix A -Coupling between sample and reference cups

The system of governing ODE's can be generalized to include heat flow on the reference side of the cell and also heat flow between the sample and reference cups and heat flow between the thermocouple and its holder environment at fixed temperature T_E. Let T_S and T_R be the sample and reference temperatures and $T_{X,Y}$ be the Y (cup (C), thermocouple (T) or thermocouple holder (H)) temperature on the X (S or R) side of the DTA . Let T_W be the furnace wall temperature with T_W = constant + αt.

We include time constants, $t_{X,Y}$ that characterize the various heat flows. In particular a time constant $t_{S,R}$ characterizes the heat flow between the two cups on the sample and reference sides of the cell. A constant $R' = m_C C^C_p / m_T C^T_p$ is defined identically for both sides.

A system of ordinary differential inhomogeneous equations applies,

$$\begin{bmatrix} m_S H_S(t)\dot{T}_S \\ \dot{T}_{S,C} \\ \dot{T}_{S,T} \\ m_R H_R(T_R)\dot{T}_R \\ \dot{T}_{R,C} \\ \dot{T}_{R,T} \end{bmatrix}$$

$$-\begin{bmatrix} -m_C C_p^C / t_{S,C} & m_C C_p^C / t_{S,C} & 0 & 0 & 0 & 0 \\ 1/t_{S,C} & -(1/t_{S,C} + 1/t_{W,C} + 1/t_{S,R}) & 1/R' t_{T,C} & 0 & 1/t_{S,R} & 0 \\ 0 & 1/t_{T,C} & -(1/t_{T,H} + 1/t_{T,C}) & 0 & 0 & 0 \\ 0 & 0 & 0 & -m_C C_p^C / t_{R,C} & m_C C_p^C / t_{R,C} & 0 \\ 0 & 1/t_{S,R} & 0 & 1/t_{R,C} & -(1/t_{R,C} + 1/t_{W,C} + 1/t_{S,R}) & 1/R'd \\ 0 & 0 & 0 & 0 & 1/t_{T,C} & -(1/t_{T,H} + 1/t_{T,C}) \end{bmatrix} \begin{bmatrix} T_S \\ T_{S,C} \\ T_{S,TC} \\ T_R \\ T_{R,C} \\ T_{R,TC} \end{bmatrix}$$

$$= \begin{bmatrix} 0 \\ T_W(t)/t_{W,C} \\ T_E / t_{T,H} \\ 0 \\ T_W(t)/t_{W,C} \\ T_E / t_{T,H} \end{bmatrix}$$

For large $t_{S,R}$ values, the first three equations decouple from the last three. Equation [1] can be obtained by letting $R'=\infty$ for small thermocouple mass and $t_{T,H}=\infty$ if heat flow down the thermocouple support rods is neglected.

Appendix B- Solution after Completion of Melting

The time constants are

$$\begin{cases} r_1 = -1/t_{T,C} \\ r_2 = \dfrac{-(t_{W,C} + t_{S,C}R + t_{W,C}R) - \sqrt{(t_{W,C} + t_{S,C}R + t_{W,C}R)^2 - 4t_{S,C}t_{W,C}R}}{2t_{S,C}t_{W,C}R} \\ r_3 = \dfrac{-(t_{W,C} + t_{S,C}R + t_{W,C}R) + \sqrt{(t_{W,C} + t_{S,C}R + t_{W,C}R)^2 - 4t_{S,C}t_{W,C}R}}{2t_{S,C}t_{W,C}R} \end{cases}$$

The temperatures are

$$\begin{cases} T_S = T_M + \alpha t + \dfrac{B}{1 + t_{S,C}Rr_2}\exp[r_2(t - t_M)] \\ \qquad + \dfrac{C}{1 + t_{S,C}Rr_3}\exp[r_3(t - t_M)] \\ T_C = T_M + \alpha(t + t_{S,C}R) + B\exp[r_2(t - t_M)] \\ \qquad + C\exp[r_3(t - t_M)] \\ T_T = T_M + \alpha(t + t_{S,C}R - t_{T,C}) + A\exp[r_1(t - t_M)] + \\ \qquad \dfrac{B}{1 + t_{T,C}r_2}\exp[r_2(t - t_M)] + \dfrac{C}{1 + t_{T,C}r_3}\exp[r_3(t - t_M)] \end{cases}$$

where

$$\begin{cases} A = G - H - \dfrac{t_{W,C}\alpha\, t_M}{t_{S,C} + t_{W,C}} - \dfrac{B}{(1 + t_{T,C}r_2)} - \dfrac{C}{(1 + t_{T,C}r_3)} \\ B = \dfrac{(1 + t_{S,C}Rr_2)\left\{(t_{S,C} + t_{W,C})F + t_{S,C}\alpha\, t_M\left[1 + (t_{S,C} + t_{W,C})Rr_3\right]\right\}}{t_{S,C}(t_{S,C} + t_{W,C})R(r_2 - r_3)} \\ C = -\dfrac{(1 + t_{S,C}Rr_3)\left\{(t_{S,C} + t_{W,C})F + t_{S,C}\alpha\, t_M\left[1 + (t_{S,C} + t_{W,C})Rr_2\right]\right\}}{t_{S,C}(t_{S,C} + t_{W,C})R(r_2 - r_3)} \end{cases}$$

with

$$\begin{cases} F = \dfrac{t_{S,C}{t_{W,C}}^2\alpha}{(t_{S,C} + t_{W,C})^2}\left[1 - \exp\left[-\left[\dfrac{1}{t_{S,C}} + \dfrac{1}{t_{W,C}}\right]t_M\right]\right] \\ G = \dfrac{t_{S,C}t_{W,C}F}{t_{S,C}t_{W,C} - t_{S,C}t_{T,C} - t_{W,C}t_{T,C}} \\ H = \dfrac{{t_{W,C}}{t_{T,C}}^2\alpha}{t_{S,C}t_{W,C} - t_{S,C}t_{T,C} - t_{W,C}t_{T,C}}\left\{1 - \exp\left[-\left(\dfrac{t_M}{t_{T,C}}\right)\right]\right\} \end{cases}$$

Nomenclature for Heat Flow Model

α	furnace wall heating rate (K/s)
ΔT	DTA signal: $\Delta T = T_T - T_W$ (K)
A^{peak}	"area" of DTA signal (K s) or (K^2)
$A_{X,Y}$	"effective" area for heat flow between X and Y (m^2)
C_0	bulk composition of the sample (mass fraction)
C_{p_C}	sample cup heat capacity (J/(kg K))
$C_{p_{S0}}$	heat capacity of sample prior to melting
C_{p_T}	thermocouple heat capacity (J/(kg K))
$h_{X,Y}$	heat transfer coefficient between X and Y (J/(K s m^2))
H_R	enthalpy of reference (J/kg)
H_S	enthalpy of sample (J/kg)
k	partition coefficient
l_{id}	extradendritic diffusion length (m)
L	latent heat (J/kg)
m	liquidus slope (K/mass fraction)
m_C	sample cup mass (kg)
m_S	sample mass (kg)
m_T	thermocouple mass (kg)
R	heat capacity ratio between sample prior to melting and sample cup
R'	heat capacity ratio between thermocouple and sample cup
t	time (s)
t^*	time at intersection of thermocouple temperature asymptote with extrapolated thermocouple temperature prior to melting (s)
t_M	melting time (s)
$t_{S,C}$	response time of heat flow between sample and sample cup (s)
$t_{W,C}$	response time of heat flow between furnace wall and sample cup (s)
$t_{T,H}$	response time of heat flow between thermocouple and thermocouple holder (s)
$t_{T,C}$	response time of heat flow between thermocouple and sample cup (s)
$t_{S,R}$	response time of heat flow between reference cup and sample cup (s)
T_C	sample cup temperature (K)
T_E	thermocouple support environment temperature (K)
T_{Liq}	liquidus temperature (K)
T_M	melting temperature of sample (K)
T_R	reference temperature (K)
$T_{R,C}$	reference cup temperature (K)
$T_{R,T}$	reference thermocouple temperature (K)
T_S	sample temperature (K)
$T_{R,C}$	sample cup temperature (K) (in Appendix A)
$T_{R,T}$	sample thermocouple temperature (K) (in Appendix A)
T_{Sol}	solidus temperature (K)
T_T	thermocouple temperature (K)
T_W	furnace wall temperature (K)
T_T^{asymp}	asymptotic approximation of thermocouple temperature during melting (K)
T_T^{extrap}	thermocouple temperature at t^* (K)
T_T^{onset}	begin of deviation of thermocouple temperature after begin of melting (K)
T_T^{peak}	peak temperature of the thermocouple (K)

Additional Nomenclature for Kinetic Models

Γ	ratio of liquid-solid surface energy to the heat of fusion
λ_2	secondary dendrite arm spacing (m)
$<C_L>$	average extradendritic liquid concentration (mass fraction)
$<C_S>$	average solid composition (mass fraction)
C_L	concentration of the liquid phase (mass fraction)
C_S	concentration of the solid phase (mass fraction)
D_L	diffusion coefficient in the liquid phase (m^2/s)
D_S	diffusion coefficient in the solid phase (m^2/s)
f_g	fraction of grain
f_s	fraction solid
F_o	fourier Number for melting
l_{id}	extradendritic diffusion length (m)
n	geometric factor
p	degree of polynomial for solute profile during melting
r	position in solid phase
r_0	position of the melting interface
R_g	final grain size for dendrite model (m)
R_M	half distance between adjacent liquid regions within the sample for melting model (m)
t_M^{alloy}	alloy melting time (s)
T_N	nucleation temperature (K)
V	dendrite tip speed (m/s)

References

1. R. F. Speyer: *Thermal Analysis of Materials*, Marcel Dekker, Inc., New York, NY. 1994.
2. D. K. Banerjee, W. J. Boettinger, R. J. Schaefer, M. E. Williams: *Modeling of Casting, Welding and Advanced Solidification Processes, VII*, M. Cross & J. Campbell, eds., TMS, Warrendale, PA, 1995, pp. 491-498.
3. A.D. Cunningham and F.W. Wilburn: *Differential Thermal Analysis, Vol.1*, R.C. Mackenzie, ed., Academic Press, London, UK, 1970, pp. 31-62.
4. A.P. Gray: *Analytical Calorimetry, Vol.1*, R.S. Porter and J.F. Johnson, eds., Plenum Press, New York, NY, 1968, pp. 209-218.
5. W. Heyroth: *J. Thermal. Analysis*, 1986, vol. 31, pp. 61-72.
6. R.D. Shull: *Thermal Analysis in Metallurgy*, R.D. Shull and A. Joshi, eds., TMS, Warrendale, PA, 1992, pp. 95-119.
7. M.J. Vold: *Analyt. Chem.*, 1949, vol. 21, pp. 683-688.
8. N.F. Tsang: *Handbook of Differential Thermal Analysis*, W.J. Smothers and Y. Chiang, eds., Chem. Publ. Comp., New York, NY, 1966, pp. 91-123.
9. H.E. Kissinger: *Analyt. Chem.*, 1957, vol. 29, pp. 1702-1706.
10. L.V. Meisel and P.J. Cote: *Acta metall.*, 1983, vol. 31, pp. 1053-1059.
11. T. Ozawa: *J. Thermal. Analysis*, 1973, vol. 5, pp. 563-576.
12. J.H. Flynn: *J. Thermal Analysis*, 1988, vol. 34, pp. 367-381
13. J.H. Perepezko: *Thermal Analysis in Metallurgy*, R.D. Shull and A. Joshi, eds., TMS, Warrendale, PA, 1992, pp. 121-153.
14. H. Fredriksson and B. Rogberg: *Metal Science*, 1979, vol. 13, pp. 685-690.
15. H. Fredriksson: *Metals Handbook,* Vol. 15 *Casting*, 9th ed., ASM International, Metals Park, OH, 1988, pp. 182-185.
16. D.A. Porter and K.E. Easterling: *Phase Transformations in Metals and Alloys*, Van Nostrand Reinhold Company, New York, NY, 1981.
17. J. Opfermann: *Netzsch Thermokinetics Software Manual*, Netzsch.Gerätebau, Selb, Germany, 2000.
18. R.I. Wu and J.H. Perepezko: *Metall. Mater. Trans. A*, 2000, vol. 31A, pp. 497-501.
19. H.B. Dong and J.D. Hunt: *J. Thermal Analysis Calorim.*, 2001, vol. 64, pp. 167-176.
20. H.B. Dong, M.M. Shin and J.D. Hunt: "A Study of Micro-Segregation Using a Novel Single-Pan Calorimeter," *Metall. Mater. Trans. A*, in press.
21. K.-W. Moon, W.J. Boettinger, U.R. Kattner, F.S. Biancaniello and C.A. Handwerker, *J. Electron. Mater.*, 2000, vol. 29, pp. 1122-1136.
22. A.T. Dinsdale: *CALPHAD*, 1991, vol. 15, pp. 317-425.
23. N. Saunders, *Mater. Sci. Forum*, 1996, vols. 217-222, pp. 667-672.
24. N. Saunders: *Superalloys 1996*, R. D. Kissinger, D. J. Deye, D. L. Anton, A. D. Cetel, M.V Nathal, T.M. Pollock and D. A. Woodford , eds., TMS, Warrendale, PA, 1996, pp. 101-110.
25. W.J. Boettinger, U.R. Kattner and D.K. Banerjee: *Modeling of Casting, Welding and Advanced Solidification Processes VIII*, B.G. Thomas and C. Beckermann, eds., TMS, Warrendale PA, 1998, pp 159-170.
26. D. Basak, W.J. Boettinger, D. Josell, SR. Coriell, J. McClure, S. Krishnan and A. Cezairliyan, *Acta Mater.*, 1999, vol. 47, pp. 3147-3158.
27. C.Y. Wang and C. Beckermann: *Metall. Trans. A*, 1993, vol. 24A, pp. 2787-2802.